Geoderma 337 (2019) 893–905

Contents lists available at ScienceDirect

Geoderma

journal homepage: www.elsevier.com/locate/geoderma

Variations in soil temperature from 1980 to 2015 in permafrost regions on the Qinghai-Tibetan Plateau based on observed and reanalysis products

Guojie Hu[a], Lin Zhao[b,*], Ren Li[a], Xiaodong Wu[a], Tonghua Wu[a], Changwei Xie[a], Xiaofan Zhu[a,d], Youqi Su[c]

[a] Cryosphere Research Station on Qinghai-Xizang Plateau, State Key Laboratory of Cryospheric Sciences, Northwest Institute of Eco-Environment and Resources, Chinese Academy of Sciences, Lanzhou 730000, China
[b] School of Geographical Sciences, Nanjing University of Information Science & Technology, Nanjing 210000, China
[c] Key Laboratory of Land Surface Process and Climate Change in Cold and Arid Regions, Northwest Institute of Eco-Environment and Resources, Chinese Academy of Sciences, Lanzhou 730000, China
[d] University of Chinese Academy of Sciences, Beijing 100049, China

ARTICLE INFO

Keywords:
Permafrost
Soil temperature
Qinghai-Tibetan Plateau
Reanalysis product
Observation

ABSTRACT

Soil temperature is an important physical variable of soil and plays a key role in controlling the underground hydro-thermal processes in permafrost regions on the Qinghai-Tibetan Plateau (QTP). Daily soil temperatures were observed at five different vegetation cover sites (alpine wet meadow, alpine meadow, alpine steppe, alpine desert steppe and alpine desert) from 2012 to 2015 in permafrost regions on the QTP. The performance of three reanalysis soil temperature products (National Centers for Environmental Prediction Climate Forecast System and Climate Forecast System Reanalysis (CFSR), European Centre for Medium-Range Weather Forecasts interim reanalysis (ERA-Interim), and Global Land Data Assimilation System (GLDAS- NOAH)) at four depths (0–10, 10–40, 40–100 and 100–200 cm) was evaluated using the observation data. The results revealed that the CFSR soil temperature products had the best performance at most sites and that GLDAS-NOAH and Era-Interim had the poorest performance. However, the original CFSR soil temperature products underestimated the lowest temperatures. The calibration models for CFSR soil temperature products were established using the observed daily soil temperature from 2013 to 2015 and were validated with observed data from 2012. The results showed that the calibrated CFSv2 products were closer to the observations at different depths in the study sites. Moreover, we investigated the variations of seasonal and annual mean soil temperature from 1980 to 2015 at depths of 0–10, 10–40, 40–100 and 100–200 cm using the soil temperature calibration results. It was found that the soil temperatures at different depths all warmed fastest in spring, more slowly in winter and slowest in autumn at most sites. In addition, the average annual soil temperature exhibited significant warming trends in the permafrost regions on the QTP. The effect was largest with alpine desert steppe and smallest with alpine wet meadow, with statistically significant rates of 0.0599, 0.0468, 0.0438, 0.0282 and 0.0145 °C/year in alpine desert steppe, alpine desert, alpine steppe, alpine meadow and alpine wet meadow, respectively. This research provides a foundation for understanding the thermal properties of permafrost on the Qinghai-Tibetan Plateau under climate change.

1. Introduction

The Qinghai-Tibetan Plateau (QTP) is known as the “Third Pole of the Earth” because of its high altitude and large area (Han et al., 2017; Yanai and Wu, 2006; Ye and Gao, 1979), and it plays an important role in the Asian monsoon system and land-atmosphere interactions. Moreover, it is highly sensitive to climate change and is considered a controlling factor to the climate of China (Feng et al., 1998; Liu and Chen, 2000; Tang et al., 1979). Recent research indicated that permafrost occupies approximately 1.06 million km^2 of land area on the Tibetan Plateau (Zou et al., 2017). The QTP has the highest elevation and the largest permafrost area in the middle and low latitude regions of the world, and it plays an important role in the distribution of permafrost around the world (Zhao et al., 2017; Zhou et al., 2000). Permafrost is a key component of the cryosphere due to its influence on energy exchange, hydrological processes, natural hazards, carbon budgets, and

* Corresponding author.
E-mail addresses: huguojie123@126.com (G. Hu), linzhao@lzb.ac.cn (L. Zhao).

https://doi.org/10.1016/j.geoderma.2018.10.044
Received 8 June 2018; Received in revised form 27 August 2018; Accepted 28 October 2018
Available online 08 November 2018
0016-7061/ © 2018 Elsevier B.V. All rights reserved.

the greater global climate system in general (Romanovsky et al., 2010; Walvoord and Kurylyk, 2016; Wu et al., 2017), and it can respond quickly to climate change (Hansson et al., 2004; IPCC, 2007). As an important underlying surface type on the QTP, the unique and complex hydrothermal physical processes of the active layer in the permafrost regions have a large regulatory effect on the surface heating field characteristics (Li et al., 2012; Qin et al., 2006; Zhao et al., 2000). Changes in permafrost can reflect thermal changes on the ground surface, which have an important impact on climate change (Zhang et al., 2008; Zhou et al., 2000). Therefore, permafrost also feeds back on climate change and their impacts on the energy and water cycles on the QTP (Cheng and Wu, 2007).

Soil temperature plays an important role in many physical, hydrothermal, and biological processes in terrestrial ecosystems by regulating the lower boundary of mass and energy exchange between the land and atmosphere (Bond-Lamberty and Thomson, 2010; Canadell et al., 2007; Hu et al., 2016; Huang et al., 2014; Toosi et al., 2014). It is also an important indicator of climate change and a critical parameter in numerical weather forecasting and climate predicting (Holmes et al., 2008; Qian et al., 2011; Zhang et al., 2001). Permafrost change is a core issue in climate change research, and soil temperature is an important parameter for studying permafrost changes (Guo et al., 2017). Soil temperature can reflect the variation of the active layer in the permafrost (Zhao et al., 2011). The seasonal variation in the soil temperature of active layer is directly related to the heat exchange between the near-surface and the atmosphere, which affects the regional climate and changes in the atmospheric circulation of East Asia (Zhang et al., 2008). Therefore, to further study the climate change over the QTP, it is necessary to pay attention to the soil temperature of the active layer in the permafrost regions (Lachenbruch, 1994; Wang et al., 2000; Zhang et al., 2008; Zhao et al., 2004). However, the complex topography and harsh environmental conditions in the permafrost regions on the QTP make it very difficult to obtain long-term observed soil temperatures at various soil depths (Costello and Horst, 1991; Liu et al., 2015; Niu et al., 1997). Most previous studies have shown that the soil temperature warming is significant in the QTP, but there are few observation stations in the permafrost regions (Fang et al., 2018; Zhu et al., 2017). Reanalysis and land surface model data have been widely used in climate change research because of their long time series and wide coverage (Dee et al., 2011; Rodell et al., 2004; Saha et al., 2014). Reanalysis products could contain uncertainties from various assimilation processes, land surface models, quality control methods, and bias corrections (Berg et al., 2003; Smith et al., 2001). These biases would have a significant influence on the performance of the reanalysis products on the QTP (Wang and Zeng, 2012; Zhu et al., 2012; Zou et al., 2014), especially in the permafrost regions (Qin et al., 2017). Until now, assessments of reanalysis data against observations over the QTP mainly focused on meteorological variables (Wang and Zeng, 2012; You et al., 2012; Zhao et al., 2008) and soil water content (Chen et al., 2017; Qin et al., 2017) and there has been little work on reanalysis datasets for soil temperature in the permafrost regions. Therefore, it is necessary to calibrate and validate the reanalysis data before applying them in the permafrost regions on the QTP.

Studies have shown that the soil temperatures have increased significantly over the past several decades (Hao et al., 2014; Oelke et al., 2004; Yesilirmak, 2014; Zhang et al., 2001; Zhu et al., 2017) and that permafrost has degraded due to climate warming in the 20th century in the Northern Hemisphere (Harris et al., 2003; Osterkamp, 2005; Osterkamp and Romanovsky, 1999; Payette et al., 2004). The warming trend has been evident in the permafrost regions on the QTP (Cheng and Wu, 2007; Wu and Zhang, 2008). Several studies have made projections of the soil temperature in permafrost regions on the QTP, and they showed that the soil temperature in the continuous permafrost zones has increased by approximately 0.1 to 0.2 °C from 1970s to 90s. The increase was 0.2 to 0.5 °C in discontinuous permafrost zones from the 1970s to 1990s but dropped to approximately 0.1 to 0.2 °C after 1995 (Zhao et al., 2010). As the active layer thickness increases, the permafrost area shrinks, and the thickness of the permafrost decreases under climate warming on the QTP (Li et al., 2012; Zhao et al., 2010). The results indicated that the warming trend during the past decades was different in different regions and was affected by many factors such as climate, vegetation, snow cover, soil properties, hydrological conditions and geothermal gradients (Bockheim and Hall, 2002; Hinkel et al., 1997). Any change in these factors must induce changes in soil temperature (Bandopadhyay et al., 1999; Hinkel et al., 1996; Shiklomanov et al., 2010) and these changes play a significant role in climate change, availability of natural resources (Burn and Smith, 1988; Goodrich, 1978; Hinzman et al., 1991; Kane et al., 1991; Lachenbruch, 1994; Romanovsky and Osterkamp, 1995), and the soil carbon budget, and it has potentially significant consequences on a global scale (Field and Raupach, 2004). Therefore, it is important to understand the variations in soil temperature in the permafrost regions (Zhao et al., 2011). Nevertheless, there is still a lack of data concerning the long-term soil temperature records, which have been less investigated with different depths, mainly because soil temperature observation data are generally scarce in the permafrost regions on the QTP (Zhu et al., 2017). In this paper, we address three principal issues that are specifically relevant to soil temperature in the permafrost regions on the QTP: (1) evaluate the performance of the reanalysis soil temperature products at different depths; 2) establish calibration models and validate the reanalysis soil temperature products from observed data; and 3) demonstrate the variations in the seasonal and annual mean soil temperatures from 1980 to 2015 in permafrost regions on the QTP.

2. Data and methods

2.1. Data

A soil temperature network of the active layer was deployed on the QTP along the Qinghai-Tibet Highway by the Cryosphere Research Station, Chinese Academy of Sciences. Data for the current study are collected at the Liangdaohe (CN04), Tongtianhe (QT06), Wudaoliang (QT08), and Xidatan (QT09) sites in permafrost regions of QTP (Fig. 1). These five sites have different land cover types and soil characteristics. The soil temperature is collected in 30 min or 1 h intervals, and the hourly average is recorded by a CR1000 data acquisition instrument (Campbell Scientific Inc.) at different depths in the active layer with an accuracy of ± 0.5 °C (Table 1). The daily soil temperatures from these five different eco-regions from 2012 to 2015 were used here to evaluate the reanalysis data products and establish calibration models from 2013 to 2015. These models were validated against observation data from 2012. The main physiographic characteristics of these five sites are listed in Table 1.

The reanalysis data used in this paper include CFSR (CFSR and CFSv2) reanalysis data provided by NCEP (Saha et al., 2014), ERA-Interim global reanalysis data provided by ECMWF (Dee et al., 2011) and land surface model data (GLDAS-NOAH) generated from the Global Land Data Assimilation System (GLDAS-2.1), which has been developed by the National Aeronautics and Space Administration (NASA) Goddard Space Flight Center (GSFC) and the National Oceanic and Atmospheric Administration (NOAA) National Centers for Environmental Prediction (NCEP) (Rodell et al., 2004). Details of each reanalysis soil temperature data set are given in Table 2.

2.2. Methods

Due to the different time resolutions of the observation and reanalysis data, these data are first processed into daily averages before analysis. In this study, the neighboring grid method was used to match reanalysis data with observations, and the daily averaged first (0–10 cm), second (10–40 cm), third (40–100 cm) and fourth layers (100–200 cm) of the soil temperature product and observations data are

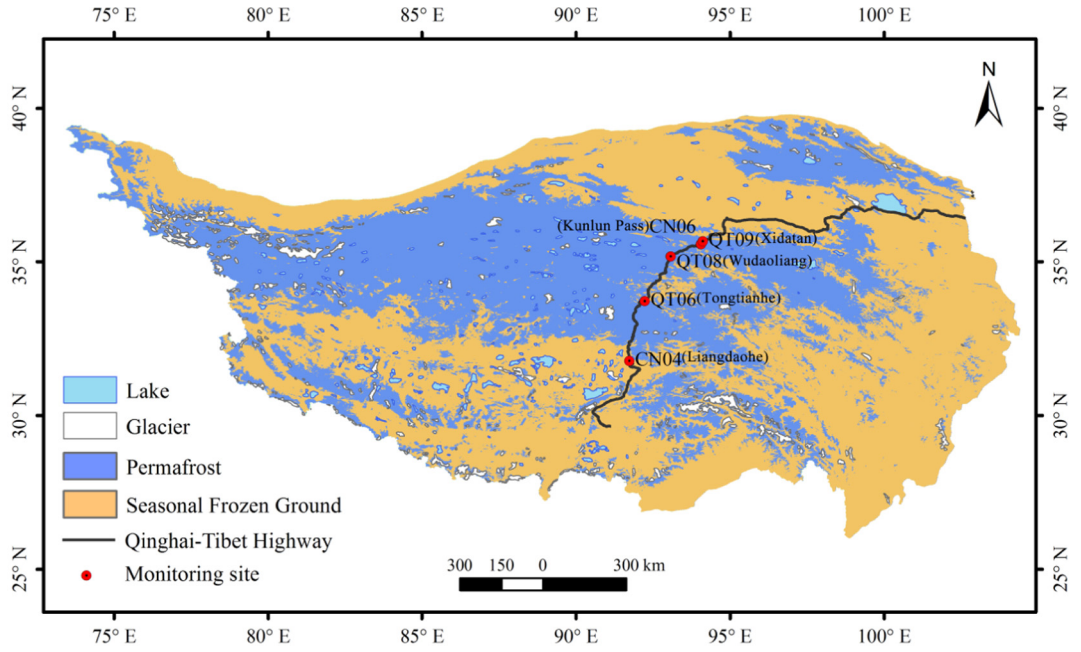

Fig. 1. Map of monitoring sites on the Tibetan Plateau.

applied (Liu et al., 2015). In addition, the comprehensive model rank (MR) (Jiang et al., 2017; You et al., 2017) that measures the consistency of simulations for each model is defined as:

$$M_R = 1 - \frac{1}{1 \times m \times n} \sum_{i=1}^{n} \text{rank}_i \quad (1)$$

where m and n is the number of models and indices, and rank_i is based on model's order of performance on each index. The M_R of the best-performing model is closer to 1, indicating higher skill (You et al., 2017).

The root mean square error (RMSE) value was used to evaluate the reanalysis products. The RMSE reflects the average deviation between the simulated and the observed values and is greater than or equal to zero. Zero is the simulated result without error, and the RMSE is calculated as:

$$RMSE = \sqrt{\frac{1}{S} \sum_{t=1}^{s} [y(t) - \hat{y}(t)]^2} \quad (2)$$

where S is the number of samples, $\hat{y}(t)(t = 1,2, \ldots,S)$ is the observed value, and $y(t)(t = 1,2, \ldots,S)$ is the simulated value. NSEE, the normalized standard error of the estimated and measured values, and Bias were used to evaluate the model. NSEE and Bias are calculated according to the following equations:

$$NSSE = \sqrt{\frac{\sum_{t=1}^{s} [y(t) - \hat{y}(t)]^2}{\sum_{t=1}^{s} [\hat{y}(t)]^2}} \quad (3)$$

$$Bias = \frac{1}{S} \sum_{t=1}^{S} |y(t) - \hat{y}(t)| \quad (4)$$

where S, $\hat{y}(t)$ and y (t) are the same as in Eq. (2).

3. Results

3.1. Reanalysis soil temperature products' performance in permafrost regions

Fig. 2 shows the daily soil temperature of different depths in the permafrost regions at CN04, CN06, QT06, QT08 and QT09 from 2013 to 2015 obtained by CFSv2, ERA-Interim and GLDAS-NOAH. It can be seen that all of the reanalysis products have well simulated the soil temperature in the first and second soil layers. The correlation coefficients were > 0.90 for all sites except CN04 in the second soil layer. The ratios of the standard deviation for all products were < 1.5, and the RMSE was < 2.0 °C, except for the ERA products for CN04 in the second soil layer (Fig. 2(a) and (b)). In the third soil layer, all products are relatively consistent at QT06 and QT08, which show that the distribution is concentrated in the Taylor diagram. However, the error was larger at other sites, especially at CN04, where the correlation coefficient was < 0.75, and the ratios of the standard deviation and RMSE were > 3.5 (Fig. 3(c)). The results also reveal that each reanalysis soil temperature products exhibit great differences in performance in the fourth soil layer, and the correlation coefficient was < 0.90 at most sites. The standard deviation ratio and RMSE of CFSv2 and GLDAS-NOAH products were > 4.0 for CN04 (Fig.3(d)). In addition, it is necessary to note that the standard deviation values of reanalysis soil temperature products were more than those of the observations for most of the models.

To synthesize the three assessment indexes an MR value (Eq. (1)) is calculated for each model to illustrate their overall ranking for the daily soil temperature at different depths in permafrost regions at all sites from 2013 to 2015 (Fig. 3). Each model is ranked from 1 (best) to 3 (worst) for each index. The length of the color column is the summary of each ranking, with shorter columns indicating better model performance. The colors represent the ranking of each individual index. The reanalysis soil temperature products have a large difference in the simulation ability of each index. It is indicated that ERA products have the best performance for all sites except QT09 in the first soil layer and have the poorest performance in the second and third soil layers. The results also reveal that CFSv2 products were lowest in error in all soil layers, except the first soil layer at all sites. The GLDAS-NOAH products were best only in the second soil layer. Overall, the best reanalysis soil temperature product for all sites is CFSv2, which achieved ten first-places. Therefore, the results of the CFSv2 soil temperature products were then utilized.

3.2. Soil temperature model calibration and validation in permafrost regions

Based on our results in Section 3.1, we further calibrated the CFSv2

Table 1
Physiographic characteristic and information of the soil temperature observation sites.

Sites	Location	Vegetation type	Longitude (°N)	Latitude (°E)	Altitude (m)	Soil temperature depth (cm)	Active layer depth (m)	Mean annual air temperature (°C)	Mean annual soil temperature (°C)	Soil classification	Drainage class
CN04	Liangdaohe	Alpine wet meadow	91.74	31.82	4808	1,8,15,28,36,50,60, 70,80,90,105,120	1.2	−2.55	−0.48	Fibristels	Very poorly
CN06	Kunlun Pass	Alpine desert	94.06	35.62	4746	10,30,50,80,100,120,140,150,160	1.65	−6.82	−3.34	Orthels	Well
QT06	Tongtianhe	Alpine steppe	92.24	33.77	4650	10,30,50,60,90,120, 150,180,200	2.5	−3.04	−0.09	Ochrepts	Somewhat Poorly
QT08	Wudaoliang	Alpine desert steppe	93.08	35.22	4783	5,10,20,40,80,120, 160, 180	2.4	−4.67	−1.98	Orthids	Well
QT09	Xidatan	Alpine meadow	94.13	35.72	4583	5,10,20,40,80,120, 140,160,180	1.35	−4.29	−1.45	Orthels	Poorly

Note: Mean annual soil temperature at 50 cm in 2012.

soil temperature products. The calibration models were established using the observed daily soil temperature from 2013 to 2015, and validated with observation data from 2012. Since the soil temperature showed similar variations among the sites, for clarity only the results from the CN06 site are discussed. The results show that the CFSv2 soil temperature products were significantly positively correlated with observations at all depths during the period 2013–2015 and correlation coefficients were 0.92, 0.96, 0.93 and 0.73 for the first, second, third and fourth soil layer, respectively (Fig. 4). The reanalysis and observed soil temperature have a good linear correlation. The calibration models between the CFSv2 product data and observations at other sites are shown in Table 3. Overall, there were stronger correlations between the daily soil temperature from the CFSv2 reanalysis dataset and observations at all sites, and the average correlations were 0.71, 0.81, 0.92 and 0.87 at all depths at CN04, QT06, QT08 and QT09, respectively.

From Fig. 6, we can see that both the original and calibrated CFSv2 products agree well with the observed temperature in the first and second soil layers at CN06 in 2012. However, the calibrated CFSv2 products show a slight improvement with the RMSE, but Bias and NSEE are much smaller. It can be seen that the original CFSv2 products underestimate in the freeze period (e.g., in Dec. and Mar.) and that the deeper the soil layer is, the greater the error is at CN06. It can be seen that the calibrated models obviously improve the accuracy in the third and fourth soil layers at CN06, especially for the lowest temperatures. After calibration, the fitting lines were much closer to the observed lines (Fig. 5). For the third soil layer, the RMSE decreased from 2.02 to 1.41 °C, the Bias decreased from −1.17 to −0.26 °C and the NSEE decreased from 0.34 to 0.24; these factors decreased from 2.29 to 1.48 °C, −0.87 to 0.14 °C and 0.57 to 0.37 in the fourth soil layer at CN06, respectively (Table 4).

The detailed information of other sites from the calibrated CFSv2 products and observations soil temperature is listed in Table 4. The results reveal that, before calibration, the other sites, whose RMSE (Eq. (2)) were > 3.3 °C, most Biases (Eq. (4)) were more than −3.26 °C, and most NSEE (Eq. (3)) values were > 0.35 in the first soil layer in 2012. After calibration, for all sites, the RMSE, Bias and NSEE in the first soil layer were < 2.32 °C, 0.56 °C and 0.40, respectively (Table 4). After calibration in the second soil layer, the calibrated CFSv2 products agree well with the observations. The average RMSE, Bias and NSEE of all sites decreased from 3.01 to 1.27 °C, −1.97 to −0.14 °C, and 0.56 to 0.23, respectively. Similar to the third and fourth soil layers, the daily soil temperatures improved greatly after calibration. The RMSE, Bias and NSEE showed a great improvement after calibration at all sites. After calibration, the RMSE, Bias and NSEE for all sites decreased on a large scale, and their averages were 1.18 °C, −0.11 °C and 0.33, and 0.78 °C, −0.02 °C and 0.34 in the third and fourth soil layers, respectively.

3.3. Trends of seasonal and annual mean soil temperature in permafrost regions

Based on the soil temperature calibrated models in Section 3.1 and observations data at CN04, CN06, QT06, QT08 and QT09, the CFSR and CFSv2 soil temperature products were revised from 1980 to 2015. Fig. 6 shows the variation of soil temperature in the first (0–10 cm), second (10–40 cm), third (4–100 cm) and fourth (100–200 cm) soil layers in spring (Mar.–May), summer (Jun.–Aug.), autumn (Sept.–Nov.), and winter (Dec.–Feb.) at CN04, CN06, QT06, QT08 and QT09 on the QTP during 1980–2015. It can be seen that the seasonal mean soil temperatures exhibit significant and similar warming trends during 1980–2015, although some differences in peaks and troughs related to inter-annual variability are noted. The results revealed that soil temperature at different depths all warmed fastest in spring, more slowly in winter and slowest in autumn at all sites, except at CN04, which had a cooling trend in spring and the fastest warming in winter. At the different soil depths, the increasing soil temperature trend in the first layer

Table 2
Information of soil temperature from reanalysis data.

Data name	Time resolution/h	Spatial resolution	Time period	Soil temperature depth/cm
CFSR	6	0.20° × 0.20°	1979–2018	0–10, 10–40, 40–100, 100–200
ERA-Interim	6	0.25° × 0.25°	1979–2018	0–7, 7–28, 28–100, 100–289
GLDAS-NOAH	3	0.25° × 0.25°	2000–2018	0–10, 10–40, 40–100, 100–200

is smaller than that in the deeper layers in spring, and these trends were 0.0814 °C/year, 0.0656 °C/year, 0.0984 °C/year and 0.0198 °C/year at CN06, QT06, QT08 and QT09, respectively (Table 5). The inter-annual variations of soil temperatures in the first soil layer are quite similar in to those in winter at CN06, QT08 and QT09. Additionally, the average annual warming rates were 0.0402 °C/year, 0.0587 °C/year and 0.0309 °C/year at CN06, QT08 and QT09, respectively. However, the average annual warming rate was significantly higher in the first soil layer than it was in deeper soil layers, and it was 0.0269 °C/year and 0.0628 °C/year at CN04 and QT06, respectively. It is notable that the warming rates during 1980–2015 of the averaged seasonal soil temperature are not warming trends in four soil layers at all sites, such as the first, second and third soil layers in spring at CN04 and the first and second soil layers in summer at QT08.

Fig. 7 shown that the annual mean soil temperatures and their long-term trends at CN04, CN06, QT06, QT08 and QT09 in the first, second, third and fourth soil layers. Although the average annual mean soil temperatures exhibit some differences, there are warming trends at all sites. The averaged warming rates among the results based on revised CFSR and CFSv2 products and observed soil temperatures were highest at QT06 and lowest at CN04 in the first soil layers (Table 5). The average warming rates of the annual mean soil temperature during 1980–2015 for all soil layers gradually decrease from QT08 to CN04, with statistically significant rates of 0.0599, 0.0468, 0.0438, 0.0282 and 0.0145 °C/year at QT08, CN06, QT06, QT09 and CN04, respectively (Table 5).

4. Discussions

4.1. Model uncertainties and possible reasons for the errors

The results presented in this study revealed that the CFSv2 daily soil

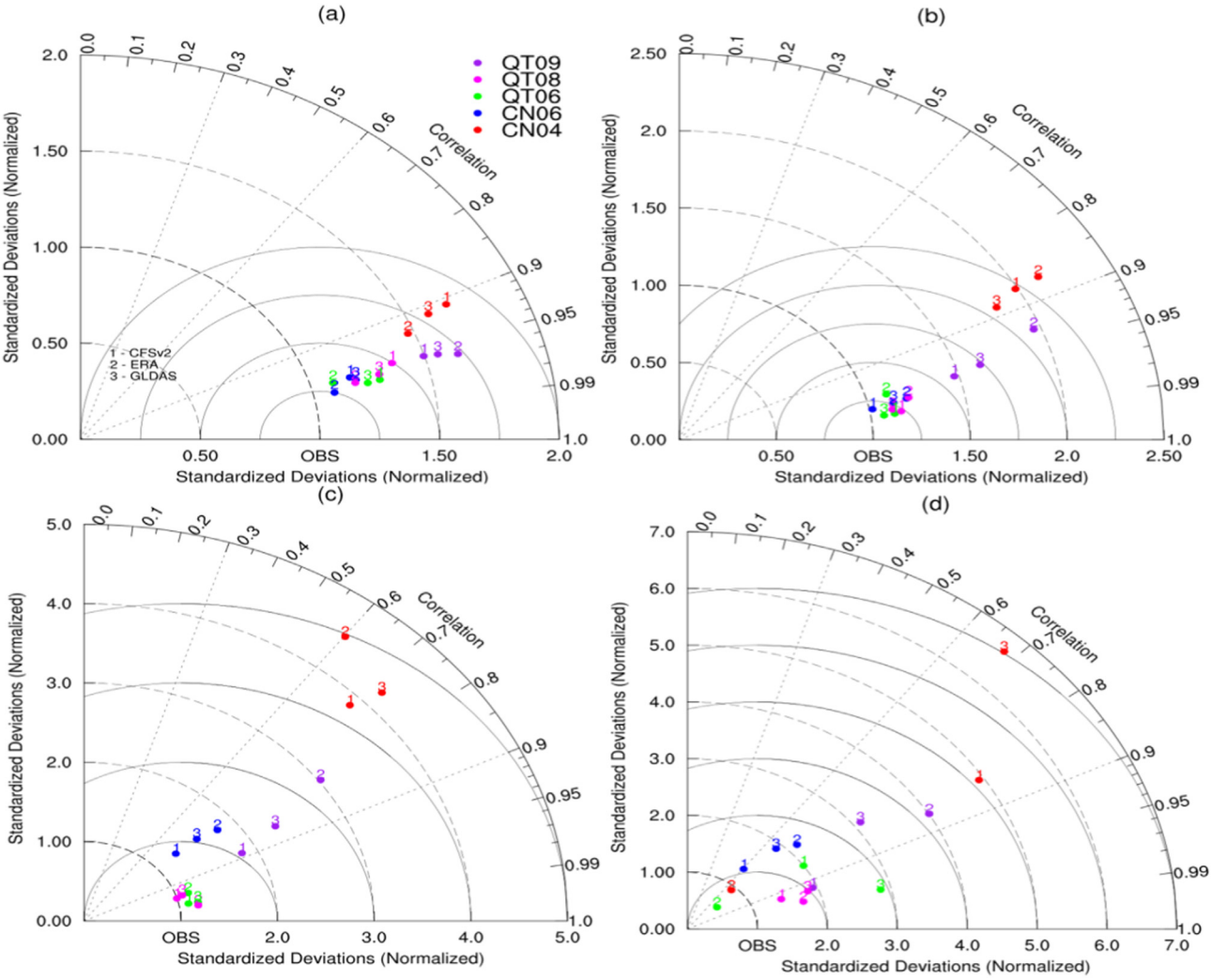

Fig. 2. Taylor program for daily soil temperature among reanalysis products with observations. (a) the first layer, (b) the second layer, (c) the third layer, (d) the fourth layer.

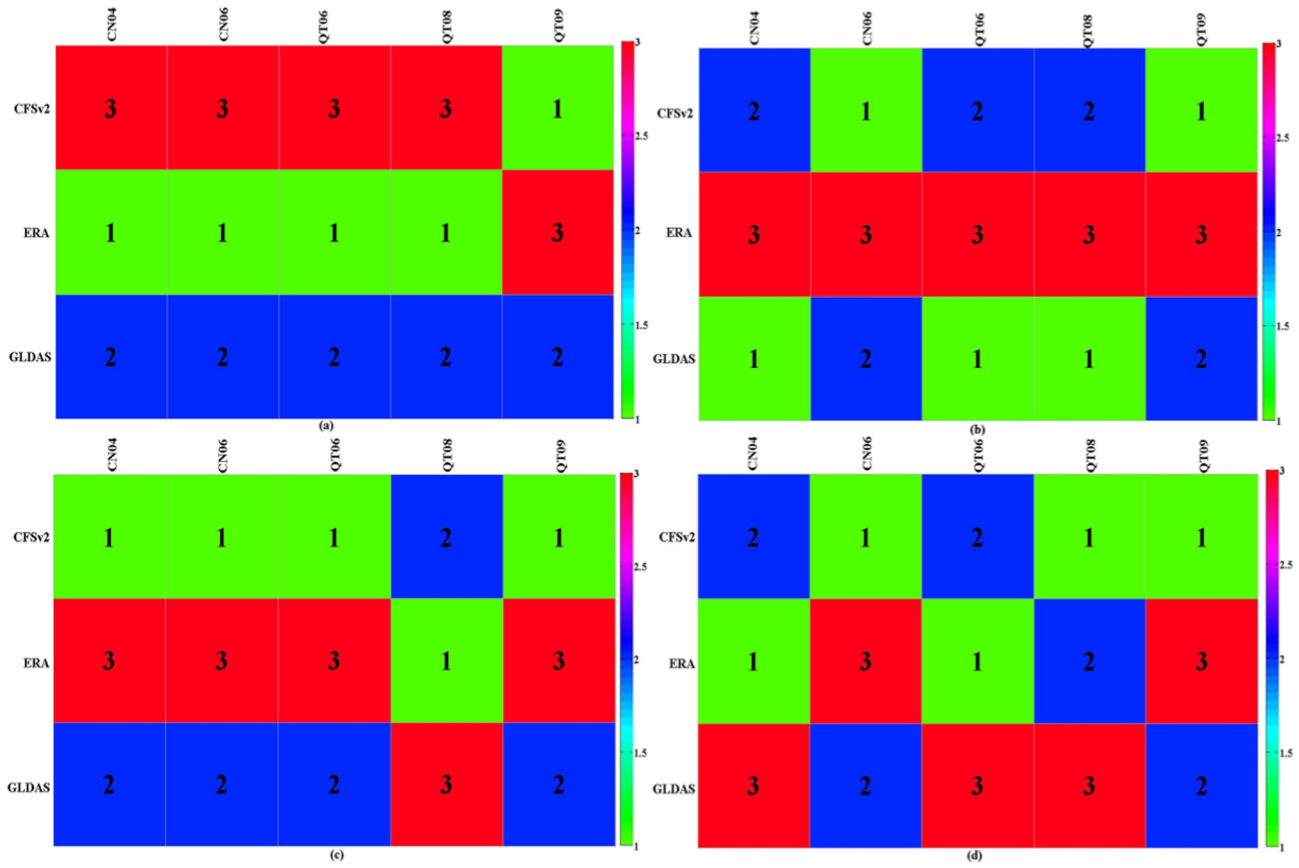

Fig. 3. The portrait diagram of the models rank based on composite rating indicator for the soil temperature of all indices. (a) the first layer, (b) the second layer, (c) the third layer, (d) the fourth layer.

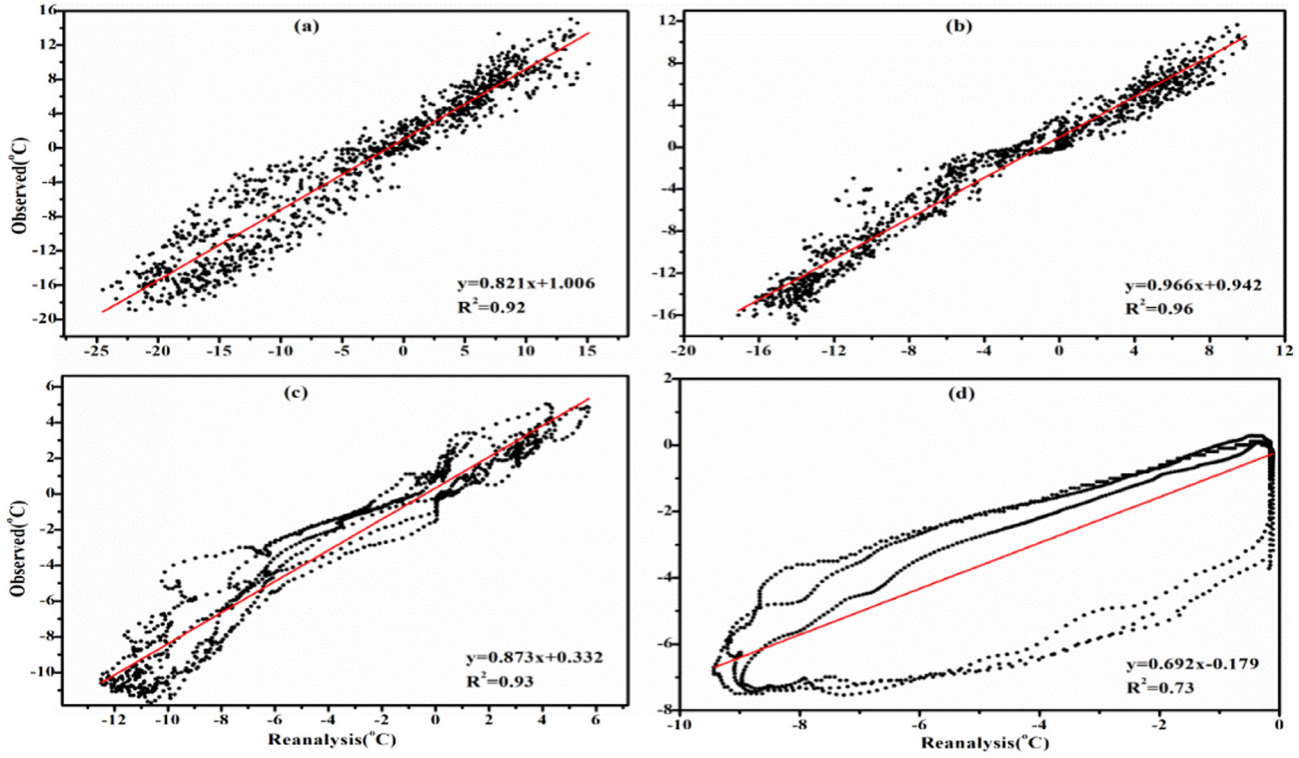

Fig. 4. Daily soil temperature observations and CFSv2 products at CN06 from 2013 to 2015. (a, the first soil layer; b, the second soil layer; c, the third soil layer; d, the fourth soil layer).

Table 3
The CFSv2 soil temperature products calibration models at different depths at all sites.

Sites	First soil layer	Second soil layer	Third soil layer	Fourth soil layer
CN04	y = 0.541x + 1.797, R^2 = 0.83	y = 0.438x + 0.858, R^2 = 0.76	y = 0.184x − 0.297, R^2 = 0.51	y = 0.172x − 0.346, R^2 = 0.72
QT06	y = 0.753x + 1.542, R^2 = 0.94	y = 0.880x + 2.051, R^2 = 0.98	y = 0.892x + 1.717, R^2 = 0.96	y = 0.414x + 0.671, R^2 = 0.69
QT08	y = 0.703x + 0.740, R^2 = 0.91	y = 0.852x + 1.333, R^2 = 0.97	y = 0.960x + 1.888, R^2 = 0.92	y = 0.646x + 0.909, R^2 = 0.87
QT09	y = 0.640x + 1.175, R^2 = 0.92	y = 0.651x + 1.022, R^2 = 0.92	y = 0.481x + 0.057, R^2 = 0.78	y = 0.479x + 0.039, R^2 = 0.86

temperature products performed best with observation data and that ERA-Interim was the worst at all sites in the permafrost regions on the QTP (Figs. 2 and 3). This was consistent with the results of Liu et al. (2015) over the QTP; however, their study was an assessment of soil temperature only in the first and second soil layers (Liu et al., 2015). Although the CFSv2 daily soil temperature products are closer to the observation data at different sites (Fig. 4 and Table 3), it can be seen that the original CFSv2 products underestimate in the freeze period, and the deeper the soil layer is, the greater the error is at CN06. This effect can be seen in the third and fourth soil layers at CN06, especially for the lowest temperatures (Fig. 5). This phenomenon is consistent with the results of other studies (Koren et al., 1999; Xiao et al., 2013); thus, the Noah land surface model is employed in both the coupled land-atmosphere model to provide a land surface prediction of surface fluxes (Ek et al., 2003), and in the Global Land Data Assimilation System, to provide land surface and evolving land states analyses (Saha et al., 2014). The land surface model was not originally developed for permafrost studies, and its ability to represent freezing and thawing processes in soil needs further enhancement (Chen et al., 2015). In the freezing period, the unfrozen water content parameterization scheme are not suitable for the permafrost on the QTP, which could limit the model' ability to satisfactory simulate soil temperature (Wu et al., 2018; Xiao et al., 2013). Therefore, the soil temperatures were underestimated by the Noah land surface model in most layers in the freeze period (Wu et al., 2018), and in the dry season in semiarid environments (Hogue et al., 2005). However, from Fig. 5 and Table 4, we can see that the soil temperature of the calibrated model is much closer to the observations, and that the underestimated temperatures in the period of freezing in the original products are efficiently improved.

In addition, it can be seen that soil temperature dropped significantly in the first, second and third soil layer in 2009 and 2010 at QT08 (Fig. 7(d)). The fluctuation is > 2.5 °C, which is significantly

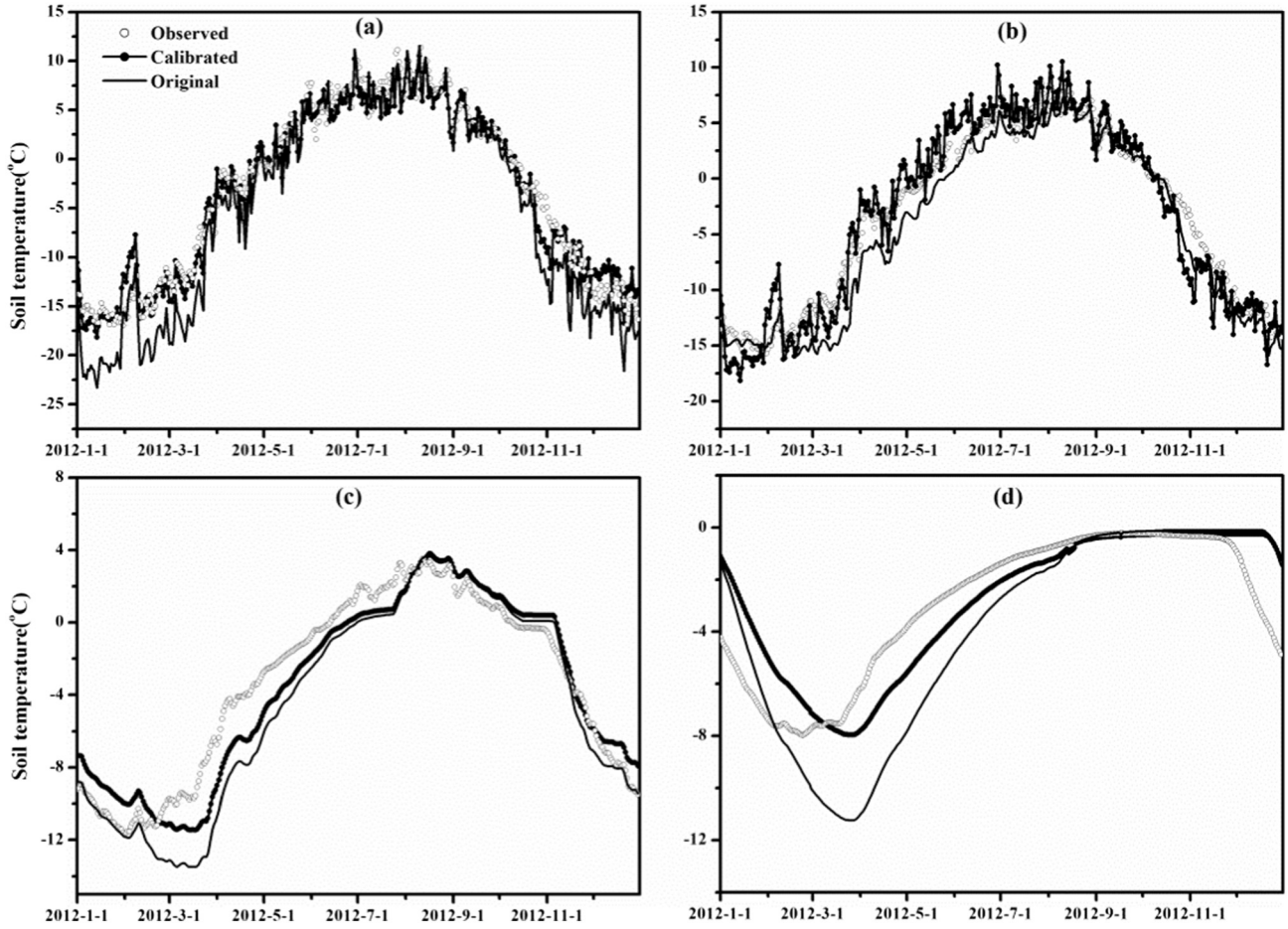

Fig. 5. Daily soil temperatures of the CFSv2 products and the observed at (a) the first soil layer, (b) the second soil layer, (c) the third soil layer, (d) the fourth soil layer at CN06 site in 2012.

Table 4
RMSE, Bias and NSEE of the reanalysis and calibrated soil temperature at different depths against the observation in 2012.

Depth	Index	Model	CN04	CN06	QT06	QT08	QT09
First layer	RMSE(°C)	Original	4.45	3.30	3.83	3.77	5.12
		Calibrated	2.32	1.92	1.99	2.12	1.77
	Bias (°C)	Original	−1.45	−2.12	−2.14	−1.29	−3.26
		Calibrated	0.42	−0.15	−0.15	0.56	−0.46
	NSEE	Original	0.77	0.35	0.51	0.46	0.84
		Calibrated	0.40	0.21	0.26	0.26	0.29
Second layer	RMSE(°C)	Original	3.76	2.08	2.65	2.42	4.13
		Calibrated	1.74	1.54	0.99	0.91	1.18
	Bias (°C)	Original	−1.29	−1.50	−2.36	−1.69	−3.01
		Calibrated	0.15	−0.54	−0.06	0.22	−0.47
	NSEE	Original	1.01	0.25	0.40	0.30	0.84
		Calibrated	0.47	0.19	0.15	0.12	0.24
Third layer	RMSE(°C)	Original	3.14	2.02	2.27	2.59	3.76
		Calibrated	0.87	1.41	0.91	1.65	1.08
	Bias (°C)	Original	−0.40	−1.17	−2.05	−1.97	−2.50
		Calibrated	0.21	−0.26	−0.10	0.08	−0.49
	NSEE	Original	2.09	0.34	0.50	0.44	1.28
		Calibrated	0.58	0.24	0.20	0.28	0.37
Fourth layer	RMSE(°C)	Original	1.86	2.29	2.55	2.72	2.71
		Calibrated	0.19	1.48	0.79	0.70	0.67
	Bias (°C)	Original	−0.32	−0.87	−1.93	−2.22	−1.88
		Calibrated	0.03	0.14	0.07	−0.09	−0.24
	NSEE	Original	2.10	0.57	1.84	0.91	1.36
		Calibrated	0.21	0.37	0.57	0.23	0.34

larger than observed in other years. Some previous studies have suggested that there is a close relationship between air and soil temperature (Cheon et al., 2014; Helama et al., 2011; Hu et al., 2017b). The results revealed that the reanalysis annual mean air temperature was significantly lower than the observed values (Fig. 8), which were − 7.20 °C and –4.21 °C, −7.21 °C and − 3.77 °C at QT08 in 2009 and 2010, respectively. The relative errors reached 70.94% and 91.15%. This could have occurred because the soil temperature was severely underestimated by CFSv2 products at QT08, which attributed to decreases in air temperature. Furthermore, errors in the model structure and model parameters may also introduce uncertainties into the simulated soil water results, which could affect the accuracy of soil temperature (Hu et al., 2015; Moradkhani et al., 2005; Qin et al., 2017). In addition, although air and soil temperature observations are used in the assimilation of CFSR soil temperature products, the observation data originate mainly from the United States and some European countries (Balsamo et al., 2015). Very few observations from Asia have been used, particularly in the permafrost regions on the QTP. Therefore, the CFSv2 products may have regional dependence, and be inapplicable outside these regions, which may be related to the topography (Rusticucci and Kousky, 2002), elevation (Ma et al., 2008), altitude (Wang et al., 2015) and the local sparsity of meteorological stations, especially on the QTP, with the notable differences of its vast area, its unique geographic setting, higher elevation and climate conditions (Qin et al., 2017).

Other possible reasons for the errors in soil temperature from reanalysis products were the differences among input parameters and parameterization schemes and the actual conditions caused the deviation in permafrost regions on the QTP (Zhou and Du, 2016). These differences include the physics, a poorly suited soil texture dataset and land cover type and local factors such as topography and drainage that were not considered in the permafrost regions (Qin et al., 2017; Wu et al., 2018). Additionally, the differences in the time used to calculate the daily mean of reanalysis (6 h) and observations (1 h), the differences in space between grid data and site data, the uncertainty of the assimilation methods and the differences in vertical levels and the assimilation method could also introduces some uncertainty into the analysis of this paper (Liu et al., 2015). It is necessary to further improve the model, especially the coupling the physical processes that were suitable for the permafrost on the QTP.

4.2. Trends of soil temperature in the permafrost regions on the QTP

The results indicate that CFSv2 daily soil temperature products obviously improve the accuracy after the calibrated models, which were established by the observation data from 2013 to 2015 at the different depths at all sites (Fig. 5 and Table 4). Therefore, the CFSR and CFSv2 soil temperature products were revised, and the trends of soil temperature from 1980 to 2015 in the permafrost regions on the QTP were analyzed. The results revealed that the soil temperature at different depths all warmed fastest in spring, more slowly in winter and slowest in autumn at most sites (Fig. 6 and Table 5). This was different for shallow soil temperatures, which also had significant variations in spring, with trends of 0.43 °C/decade, but a major variation was found for winter, with the trend of 0.57 °C/decade from 1960 to 2014 (Zhu et al., 2017). The main reason is that the previous studies primarily examined seasonal frozen soil, but this could also be associated with the freezing and thawing process in permafrost regions. According to Zhao et al. (2000), soils near the ground surface are thawed, and evaporation becomes more extensive in the daytime and soils are frozen and the water migrates upwards to the freezing front at night. The unfrozen water content and now accumulation decrease gradually during the spring warming stage (Qian et al., 2011; Zhao et al., 2000). In contrast, the thawing process that occurs in surface soil during this period tends to absorb heat from the atmosphere and transfer it downwards. This is accompanied by an increase in air temperature, thus accelerating the warming process (Hu et al., 2015; Jiao et al., 2014; Romanovsky and Osterkamp, 1997; Zhao et al., 2000). These were also possible reasons why the soil temperature rise trend in the first layer was smaller than the deeper layers in spring (Zhao et al., 2000), but not why the soil temperature warming weakened with an increase in depth (Guo et al., 2017). In contrast, there was a cooling trend in spring and significant warming in winter at CN04, which can be attributed to higher soil water content and thicker surface organic horizon; the organic horizon in this site is > 40 cm and soils are saturated during most of the growing season, thus very poorly drained. To thaw of the high ice content in the soil during the spring thaw would take a lot of energy, thus showing the cooling trend, and the larger thermal conductivity of organic matter in winter is conducive to the release of more heat from the frozen soil (Shur and Jorgenson, 2007; Xie et al., 2010). The averaged seasonal soil temperatures are not all warming trends in the

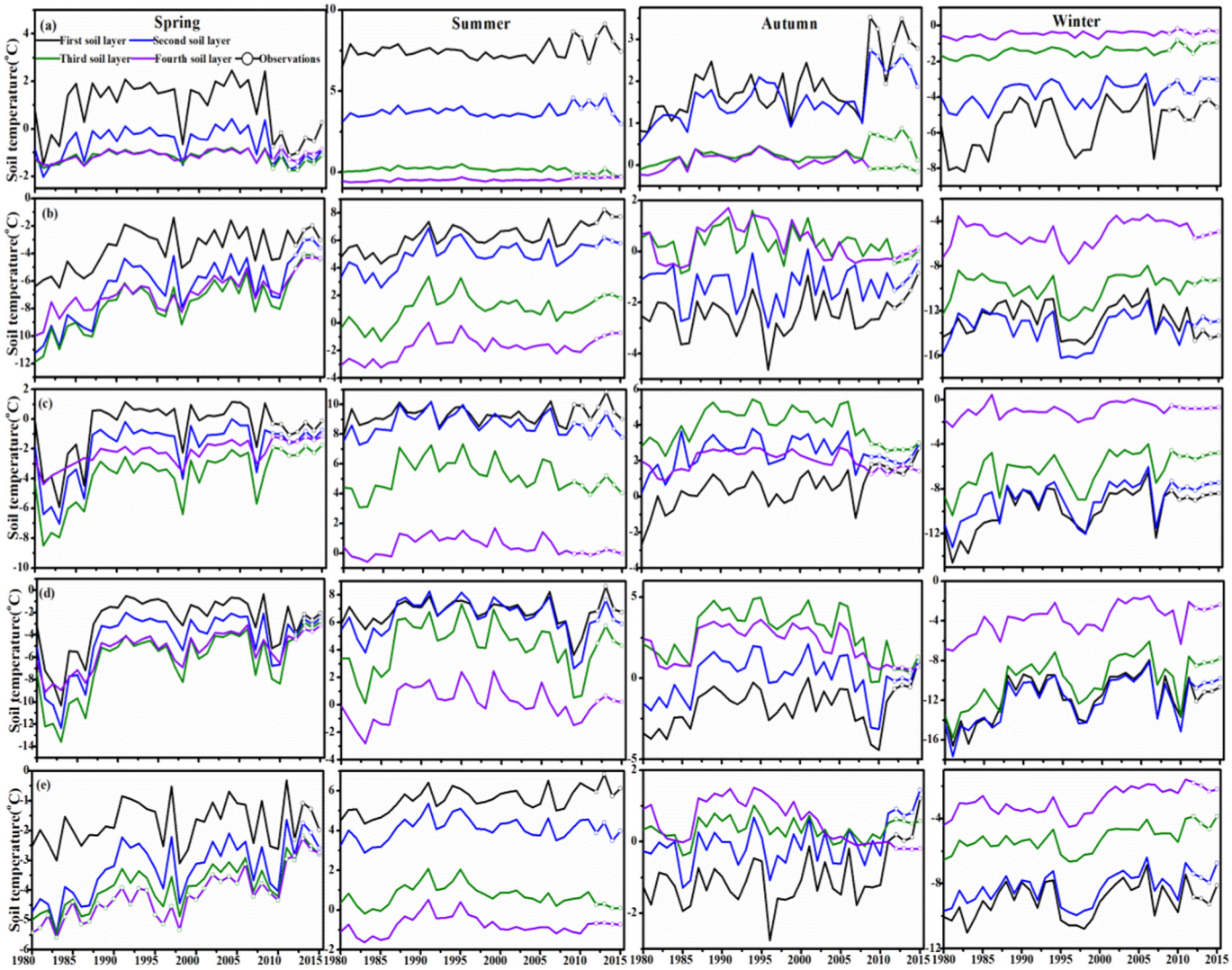

Fig. 6. The spring, summer, autumn, and winter mean soil temperature at the different soil layers on the QTP during 1980–2015. (a) CN04, (b) CN06, (c) QT06, (d) QT08, (e) QT09.

four soil layers at all sites and are related to different soil characteristics, hydro-thermal processes, local environmental conditions and reanalysis products uncertainties in the permafrost regions (Hu et al., 2017a; Pang et al., 2011).

Compared with previous studies, which found the warming rates of the annual mean soil temperature to have statistically significant rates of 0.0718, 0.0578, 0.0577, 0.0524, 0.0540, and 0.0489 °C/year at depths of 0, 5, 10, 15, 20, and 40 cm from 1983 to 2013 (Zhu et al., 2017), the temperatures in shallow (5–20 cm) and deep soils (40–320 cm) increased at 0.36 and 0.36 °C/decade, for the annual series from 1960 to 2014 on the Tibetan Plateau (Fang et al., 2018), respectively. The annual mean soil temperature warming trends were 0.0439, 0.0449, 0.0396 and 0.0259 °C/year at depths of 0–10, 10–40, 40–100 and 100–200 cm, respectively, from 1980 to 2015 in this study in permafrost regions (Table 5). The results were obviously inconsistent with previous studies, not only because they studied the average situation over the QTP but also because a few sites in the permafrost regions, generally stations of the China Meteorological Administration were located in the seasonally frozen area (Yu et al., 2003). Compared with the results of Zhu et al. (2017), it can be found that the warming rate of permafrost was not faster than that of seasonal frozen ground because of the release and absorption of heat during the freeze-thaw process of the active layer, which could reduce the annual variation in soil temperature (Zhao et al., 2004). In addition, the warming rate with permafrost was faster from 1980 than that from 1960 (Fang et al., 2018). The results indicated a regime shift to a warmer mean-state after 1997/98 (Fig. 7), similar to the result of Zhu et al. (2017), due to the major El Niño that occurred in all the time series, and the changes were consistent with the mean surface air temperature in the Northern Hemisphere (Luo et al., 2011). Further, it can be seen from Fig. 7 that the warming trend was slowed down after 2005, which was delayed compared to the global warming hiatus after the late 1990s (Trenberth and Fasullo, 2013; Zhu et al., 2017).

Among all sites, the average annual warming rates of soil temperature were highest at QT08, with alpine desert steppe, and lowest at CN04, with alpine wet meadow, with statistically significant rates of 0.0599, 0.0468, 0.0438, 0.0282 and 0.0145 °C/year at QT08, CN06, QT06, QT09 and CN04, respectively (Table 5). The results reveal that vegetation had a significant effect on the permafrost regions (Lu et al., 2006). The soil temperature variation was also restricted by other factors such as soil texture and water (Wang et al., 2014). There was more soil water and organic matter coverage at CN04, which could be beneficial for mitigating the trend of permafrost degradation caused by climate warming (Shur and Jorgenson, 2007; Wang et al., 2014). The alpine wet meadow generally has thick organic horizons which is syngenetic with permafrost aggradation. The processes and modes of

Table 5
The climatological warming rates (°C/year) of the spring, summer, autumn, winter and annual mean soil temperature at different soli layers on the QTP during 1980–2015.

Sites	Soil layers	Spring	Summer	Autumn	Winter	Annual
CN04	1	−0.0168	0.0164	0.0420	0.0660	0.0269
	2	−0.0021	0.0092	0.0337	0.0339	0.0187
	3	−0.0005	−0.0069	0.0137	0.0181	0.0061
	4	0.0078	0.0057	−0.0013	0.0091	0.0053
CN06	1	0.0814	0.0658	0.0193	−0.0056	0.0402
	2	0.159	0.0528	0.0064	0.0131	0.0578
	3	0.1458	0.0430	−0.0117	0.0261	0.0508
	4	0.1014	0.0389	−0.0198	0.0321	0.0382
QT06	1	0.0656	0.0131	0.0695	0.1028	0.0628
	2	0.0924	0.0002	0.0174	0.0853	0.0488
	3	0.1184	−0.0070	−0.0140	0.0872	0.0462
	4	0.0559	−0.0056	−0.0052	0.0251	0.0176
QT08	1	0.0984	−0.0006	0.0420	0.0951	0.0587
	2	0.1341	−0.0046	0.0132	0.1150	0.0644
	3	0.1730	0.0127	−0.0344	0.1312	0.0706
	4	0.1078	0.0158	−0.0317	0.0915	0.0459
QT09	1	0.0198	0.0342	0.0347	0.0350	0.0309
	2	0.0578	0.0103	0.0256	0.0455	0.0348
	3	0.0569	−0.0078	0.0015	0.0471	0.0244
	4	0.0649	0.0018	−0.0308	0.0547	0.0227

All of the linear trends are statistically significant ($p < 0.05$).

permafrost degradation were the similar to those in the permafrost regions in the Mahan Mountain in the Loess Plateau (Xie et al., 2010). In addition, the results revealed that the warming rates of soil temperature alpine desert steppe at QT08 were higher than those in alpine desert at CN06. Thus, the observed annual soil water content at different depths at CN06 was significantly higher than that at QT08 in 2013 (Fig. 9), which has a cooling effect on soil temperature in the warm season (Zhou et al., 2000). Further, there were 8.8% and 7.5% (< 0.054 mm) fine particle components at CN06 and QT08, respectively. The higher the content of fine-grained particles is, the more water is retained in the soil; the evaporation of water consumes heat, which causes the soil temperature warming trend to decrease (Li et al., 2012). Our results also demonstrate that the soil temperature warming trend was obviously lower in warm permafrost than in cold permafrost (Cheng and Wu, 2007; Li et al., 2012; Osterkamp, 2007), consistent with the results of Gao and Wu (2015), who showed that the rise in soil temperatures for warm permafrost under the natural ground was approximately 0.022 and 0.048 °C/year for cold permafrost along the Qinghai-Xizang Highway from 1996 to 2012, which was close to the results of CN04 and CN06. The results were also the same as those of a previous study in the Urengoy region of Russia, which indicated that the rise rate of soil temperature in warm and cold permafrost regions reaches 0.045 and 0.030 °C/year, respectively (Romanovsky et al., 2010). This may be because the unfrozen water content was significantly smaller and there is a lower phase change heat in cold permafrost than in warm permafrost (Wu et al., 2009). Similarly, the soil temperature at 10 cm depth warmed at an average rate of 0.031 °C/year from 1967 to 2002 in North America (Hu and Feng, 2003). However, in all of Canada, the annual mean soil temperature at a 20 cm depth increased by 0.06 °C/year using process-based model results from 1901 to 1995 (Zhang et al., 2005).

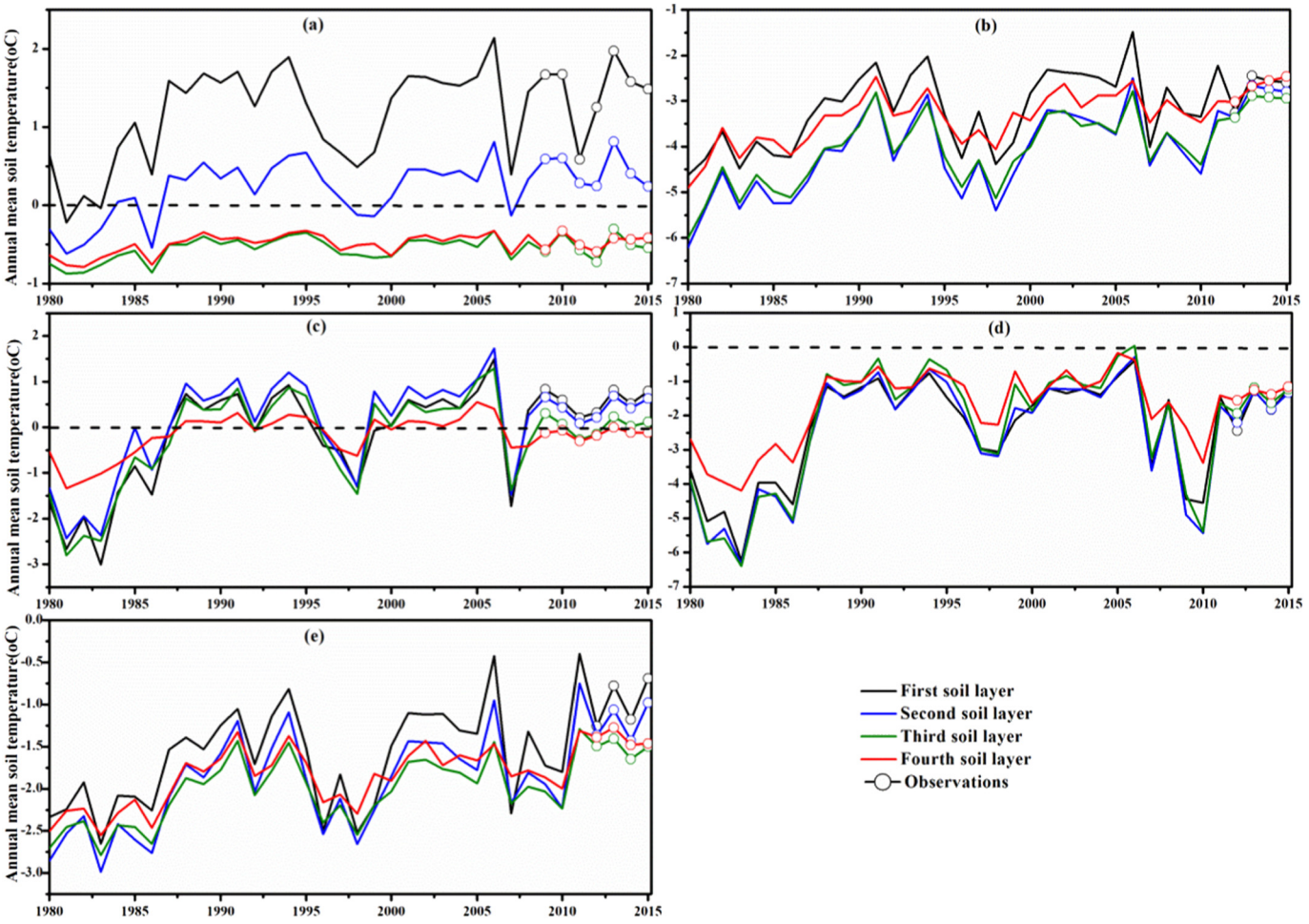

Fig. 7. Time series of the annual mean soil temperature at the different soil layers on the QTP during 1980–2015. (a) CN04, (b) CN06, (c) QT06, (d) QT08, (e) QT09.

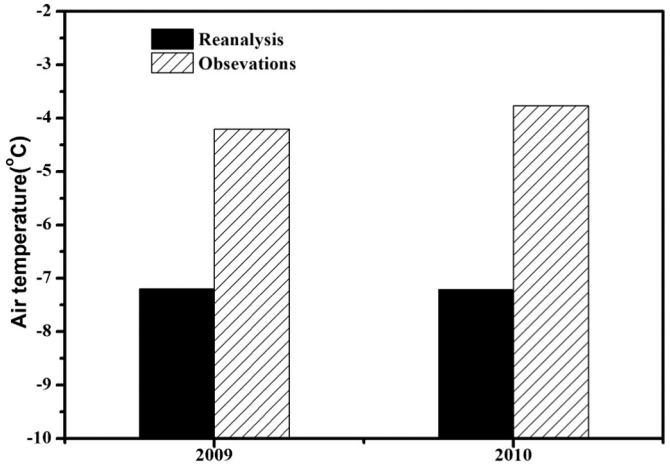

Fig. 8. The reanalysis and observations annual mean air temperature at QT08 during 2009–2010.

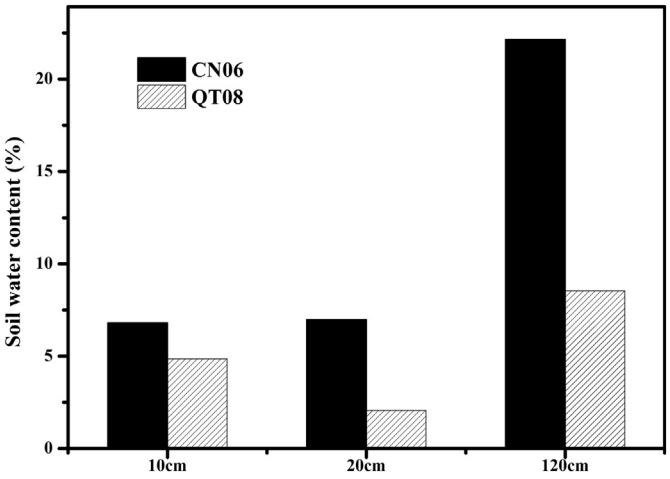

Fig. 9. The observation annual soil water content with different depths at CN06 and QT08 in 2013.

5. Conclusions

In this study, we first evaluated three reanalysis soil temperature products at four depth increments against the observed data at representative sites of different land cover types in the permafrost regions on the QTP. The results revealed that the CFSv2 products had the lowest error at most sites in the four soil layers (0–10, 10–40, 40–100 and 100–200 cm) and were the best reanalysis soil temperature products for all sites, with ten first-places ranking. There were stronger correlations between the daily soil temperature from the CFSv2 reanalysis dataset and observations at all sites. Then, we established the soil temperature calibrated models using the observation data from 2013 to 2015. The results showed that the calibrated CFSv2 products were closer to the observations at different depths in the study region. Based on the soil temperature calibration results, we examined the trends of seasonal and annual mean soil temperatures at depths of 0–10, 10–40, 40–100 and 100–200 cm from 1980 to 2015 in permafrost regions. The results showed that the soil temperature at different depths all warmed fastest in spring, slowly in winter and slowest in autumn at all sites, except at CN04, which has a cooling trend in spring and the fastest warming in winter. The inter-annual variations of soil temperatures in the first soil layer are quite similar in winter at CN06, QT08 and QT09. The average annual warming rates were 0.0402 °C/year, 0.0587 °C/year and 0.0309 °C/year at CN06, QT08 and QT09, respectively. Significant warming trends of the average annual soil temperature were detected in the permafrost regions on the QTP from 1980 to 2015. The highest was at QT08 with alpine desert steppe and lowest at CN04 with alpine wet meadow, with statistically significant rates of 0.0599, 0.0468, 0.0438, 0.0282 and 0.0145 °C/year at QT08, CN06, QT06, QT09 and CN04, respectively. The results also show that the CFSv2 reanalysis soil temperature products have larger errors at some sites due to the Noah land surface model was not originally developed for permafrost studies and the model structure and model parameters may bring uncertainties. Therefore, efforts to improve the model by coupling physical processes and research on the spatial difference of the soil warming trend in the permafrost regions on the QTP is expected to continue for the foreseeable future.

Acknowledgements

This work was financially supported by the Strategic Priority Research Program of Chinese Academy of Sciences (XDA20020102), the Science Fund for Creative Research Groups of National Natural Science Foundation of China (41721091), the National Natural Science Foundation of China (41601078, 41871060, 41690142, 41671070, 41771076), and the Excellent Youth Scholars of Northwest Institute of Eco-Environment and Resources.

References

Balsamo, G., Albergel, C., Beljaars, A., Boussetta, S., Brun, E., Cloke, H., Dee, D., Dutra, E., Munoz-Sabater, J., Pappenberger, F., de Rosnay, P., Stockdale, T., Vitart, F., 2015. ERA-interim/land: a global land surface reanalysis data set. Hydrol. Earth Syst. Sci. 19 (1), 389–407.

Bandopadhyay, S., Ke, J., Nelson, M.G., Chen, G., Izaxon, V., 1999. Analysis and prediction of water infiltration in underground, frozen placer mines. In: Mining in the Arctic, pp. 71–78.

Berg, A.A., Famiglietti, J.S., Walker, J.P., Houser, P.R., 2003. Impact of bias correction to reanalysis products on simulations of North American soil moisture and hydrological fluxes. J. Geophys. Res.-Atmos. 108 (D16).

Bockheim, J.G., Hall, K.J., 2002. Permafrost, active-layer dynamics and periglacial environments of continental Antarctica: periglacial and permafrost research in the southern hemisphere. S. Afr. J. Sci. 98 (1 & 2), 82–90.

Bond-Lamberty, B., Thomson, A., 2010. Temperature-associated increases in the global soil respiration record. Nature 464 (7288), 579–U132.

Burn, C., Smith, C., 1988. Observations of the "thermal offset" in near-surface mean annual ground temperatures at several sites near Mayo, Yukon Territory, Canada. Arctic 99–104.

Canadell, J.G., Le Quere, C., Raupach, M.R., Field, C.B., Buitenhuis, E.T., Ciais, P., Conway, T.J., Gillett, N.P., Houghton, R.A., Marland, G., 2007. Contributions to accelerating atmospheric CO(2) growth from economic activity, carbon intensity, and efficiency of natural sinks. Proc. Natl. Acad. Sci. U. S. A. 104 (47), 18866–18870.

Chen, H., Nan, Z., Zhao, L., Ding, Y., Chen, J., Pang, Q., 2015. Noah modelling of the permafrost distribution and characteristics in the west Kunlun area, Qinghai-Tibet Plateau, China. Permafr. Periglac. Process. 26 (2), 160–174.

Chen, Y., Yang, K., Qin, J., Cui, Q., Lu, H., La, Z., Han, M., Tang, W., 2017. Evaluation of SMAP, SMOS, and AMSR2 soil moisture retrievals against observations from two networks on the Tibetan plateau. J. Geophys. Res.-Atmos. 122 (11), 5780–5792.

Cheng, G., Wu, T., 2007. Responses of permafrost to climate change and their environmental significance, Qinghai-Tibet Plateau. J. Geophys. Res. Earth Surf. 112 (F2).

Cheon, J.-Y., Ham, B.-S., Lee, J.-Y., Park, Y., Lee, K.-K., 2014. Soil temperatures in four metropolitan cities of Korea from 1960 to 2010: implications for climate change and urban heat. Environ. Earth Sci. 71 (12), 5215–5230.

Costello, T.A., Horst, W.J., 1991. Soil-temperature sensor installation - a comparison of 2 methods. Trans. ASAE 34 (3), 904–908.

Dee, D.P., Uppala, S.M., Simmons, A.J., Berrisford, P., Poli, P., Kobayashi, S., Andrae, U., Balmaseda, M.A., Balsamo, G., Bauer, P., Bechtold, P., Beljaars, A.C.M., van de Berg, L., Bidlot, J., Bormann, N., Delsol, C., Dragani, R., Fuentes, M., Geer, A.J., Haimberger, L., Healy, S.B., Hersbach, H., Holm, E.V., Isaksen, L., Kallberg, P., Koehler, M., Matricardi, M., McNally, A.P., Monge-Sanz, B.M., Morcrette, J.J., Park, B.K., Peubey, C., de Rosnay, P., Tavolato, C., Thepaut, J.N., Vitart, F., 2011. The ERA-interim reanalysis: configuration and performance of the data assimilation system. Q. J. R. Meteorol. Soc. 137 (656), 553–597.

Ek, M., Mitchell, K., Lin, Y., Rogers, E., Grunmann, P., Koren, V., Gayno, G., Tarpley, J., 2003. Implementation of Noah land surface model advances in the National Centers for Environmental Prediction operational mesoscale Eta model. J. Geophys. Res. Atmos. 108 (D22), 1–16.

Fang, X., Luo, S., Lyu, S., 2018. Observed soil temperature trends associated with climate change in the Tibetan Plateau, 1960–2014. Theor. Appl. Climatol. 1–13.

Feng, S., Tang, M., Wang, D., 1998. New evidence for the Qinghai-Xizang(Tibet) Plateau as a pilot region of climatic fluctuation in China. Chin. Sci. Bull. 43 (6), 1745–1749.

Field, C.B., Raupach, M., 2004. Toward CO2 Stabilization: Issues, Strategies, and Consequences. Island Press, Washington, DC.

Gao, S., Wu, Q., 2015. Period analysis and trend forecast for soil temperature in the Qinghai-Xizang Highway by wavelet transformation. Environ. Earth Sci. 74 (4), 2883–2891.
Goodrich, L., 1978. Some Results of a Numerical Study of Ground Thermal Regimes.
Guo, D., Li, D., Liu, G., 2017. Simulated change in soil temperature on the Tibetan Plateau from 1901 to 2010. J. Quat. Sci. 37 (5), 1102–1110.
Han, C., Ma, Y., Chen, X., Su, Z., 2017. Trends of land surface heat fluxes on the Tibetan Plateau from 2001 to 2012. Int. J. Climatol. 37 (14), 4757–4767.
Hansson, K., Šimůnek, J., Mizoguchi, M., Lundin, L.-C., Van Genuchten, M.T., 2004. Water flow and heat transport in frozen soil. Vadose Zone J. 3 (2), 693–704.
Hao, G., Zhuang, Q., Pan, J., Jin, Z., Zhu, X., Liu, S., 2014. Soil thermal dynamics of terrestrial ecosystems of the conterminous United States from 1948 to 2008: an analysis with a process-based soil physical model and AmeriFlux data. Clim. Chang. 126 (1–2), 135–150.
Harris, C., Vonder Muhll, D., Isaksen, K., Haeberli, W., Sollid, J.L., King, L., Holmlund, P., Dramis, F., Guglielmin, M., Palacios, D., 2003. Warming permafrost in European mountains. Glob. Planet. Chang. 39 (3–4), 215–225.
Helama, S., Tuomenvirta, H., Venalainen, A., 2011. Boreal and subarctic soils under climatic change. Glob. Planet. Chang. 79 (1–2), 37–47.
Hinkel, K.M., Nelson, F.E., Shur, Y., Brown, J., Everett, K.R., 1996. Temporal changes in moisture content of the active layer and near-surface permafrost at Barrow, Alaska, USA: 1962–1994. Arct. Alp. Res. 28 (3), 300–310.
Hinkel, K.M., Outcalt, S.I., Taylor, A.E., 1997. Seasonal patterns of coupled flow in the active layer at three sites in northwest North America. Can. J. Earth Sci. 34 (5), 667–678.
Hinzman, L., Kane, D., Gieck, R., Everett, K., 1991. Hydrologic and thermal properties of the active layer in the Alaskan Arctic. Cold Reg. Sci. Technol. 19 (2), 95–110.
Hogue, T.S., Bastidas, L., Gupta, H., Sorooshian, S., Mitchell, K., Emmerich, W., 2005. Evaluation and transferability of the Noah land surface model in semiarid environments. J. Hydrometeorol. 6 (1), 68–84.
Holmes, T.R.H., Owe, M., De Jeu, R.A.M., Kooi, H., 2008. Estimating the soil temperature profile from a single depth observation: a simple empirical heatflow solution. Water Resour. Res. 44 (2), 1–11.
Hu, Q., Feng, S., 2003. A daily soil temperature dataset and soil temperature climatology of the contiguous United States. J. Appl. Meteorol. 42 (8), 1139–1156.
Hu, G., Zhao, L., Li, R., Wu, T., Wu, X., Pang, Q., Xiao, Y., Qiao, Y., Shi, J., 2015. Modeling hydrothermal transfer processes in permafrost regions of Qinghai-Tibet Plateau in China. Chin. Geogr. Sci. 25 (6), 713–727.
Hu, G., Zhao, L., Wu, X., Li, R., Wu, T., Xie, C., Qiao, Y., Shi, J., Li, W., Cheng, G., 2016. New Fourier-series-based analytical solution to the conduction-convection equation to calculate soil temperature, determine soil thermal properties, or estimate water flux. Int. J. Heat Mass Transf. 95, 815–823.
Hu, G., Zhao, L., Wu, X., Li, R., Wu, T., Xie, C., Pang, Q., Zou, D., 2017a. Comparison of the thermal conductivity parameterizations for a freeze-thaw algorithm with a multi-layered soil in permafrost regions. Catena 156, 244–251.
Hu, G., Zhao, L., Wu, X., Wu, T., Li, R., Xie, C., Xiao, Y., Pang, Q., Liu, G., Hao, J., Shi, J., Qiao, Y., 2017b. A mathematical investigation of the air-ground temperature relationship in permafrost regions on the Tibetan Plateau. Geoderma 306, 244–251.
Huang, F., Zhan, W., Ju, W., Wang, Z., 2014. Improved reconstruction of soil thermal field using two-depth measurements of soil temperature. J. Hydrol. 519, 711–719.
IPCC, 2007. Climate Change Synthesis Report. (Cambridge).
Jiang, S., Jiang, Z., Li, W., Shen, Y., 2017. Evaluation of the extreme temperature and its trend in China simulated by CMIP5 models. In: Progressus Inquisitiones de Mutatione Climatis. 13(1). pp. 11–24.
Jiao, Y., Li, R., Zhao, L., Wu, T., Xiao, Y., Hu, G., Qiao, Y., 2014. Processes of soil thawing-freezing and features of soil moisture migration in the permafrost active layer. J. Glaciol. Geocryol. 36 (2), 237–247.
Kane, D.L., Hinzman, L.D., Zarling, J.P., 1991. Thermal response of the active layer to climatic warming in a permafrost environment. Cold Reg. Sci. Technol. 19 (2), 111–122.
Koren, V., Schaake, J., Mitchell, K., Duan, Q.Y., Chen, F., Baker, J.M., 1999. A parameterization of snowpack and frozen ground intended for NCEP weather and climate models. J. Geophys. Res.-Atmos. 104 (D16), 19569–19585.
Lachenbruch, A.H., 1994. Permafrost, the Active Layer, and Changing Climate. US Geological Survey 2331–1258.
Li, R., Zhao, L., Ding, Y.J., Tonghua, Wu., Xiao, Y., Du, E., 2012. Temporal and spatial variations of the active layer along the Qinghai-Tibet highway in a permafrost region. Sci. Bull. 57 (35), 4609–4616.
Liu, X.D., Chen, B.D., 2000. Climatic warming in the Tibetan Plateau during recent decades. Int. J. Climatol. 20 (14), 1729–1742.
Liu, C., Yu, Y., Xie, J., Zhou, X., Li, J., Ge, J., 2015. Applicability of soil temperature and moisture in several datasets over Qinghai-Xizang Plateau. Plateau Meteorol. 34 (3), 653–665.
Lu, Z., Wu, Q., Sheng, Y., Zhang, L., 2006. Heat and water difference of active layers beneath different surface conditions near Beiluhe in Qinghai-Xizang Plateau. J. Glaciol. Geocryol. 28 (5), 642–647.
Luo, J.-J., Behera, S.K., Masumoto, Y., Yamagata, T., 2011. Impact of global ocean surface warming on seasonal-to-interannual climate prediction. J. Clim. 24 (6), 1626–1646.
Ma, L., Zhang, T., Li, Q., Frauenfeld, O.W., Qin, D., 2008. Evaluation of ERA-40, NCEP-1, and NCEP-2 reanalysis air temperatures with ground-based measurements in China. J. Geophys. Res.-Atmos. 113 (D15), 1–15.
Moradkhani, H., Hsu, K.L., Gupta, H., Sorooshian, S., 2005. Uncertainty assessment of hydrologic model states and parameters: sequential data assimilation using the particle filter. Water Resour. Res. 41 (5), 1–17.
Niu, G., Sun, S., Hong, Z., 1997. Numerical simulation on water and heat transport in the desert soil and atmospheric boundary layer. Acta Meteorol. Sin. 55 (4), 398–405.
Oelke, C., Zhang, T.J., Serreze, M.C., 2004. Modeling evidence for recent warming of the Arctic soil thermal regime. Geophys. Res. Lett. 31 (7), 1–4.
Osterkamp, T.E., 2005. The recent wan-ning of permafrost in Alaska. Glob. Planet. Chang. 49 (3–4), 187–202.
Osterkamp, T.E., 2007. Characteristics of the recent warming of permafrost in Alaska. J. Geophys. Res. Earth Surf. 112 (F2), 1–10.
Osterkamp, T.E., Romanovsky, V.E., 1999. Evidence for warming and thawing of discontinuous permafrost in Alaska. Permafr. Periglac. Process. 10 (1), 17–37.
Pang, Q., Zhao, L., Li, S., 2011. Influences of local factors on ground temperatures in permafrost regions along the Qinghai-Tibet highway. J. Glaciol. Geocryol. 33 (2), 349–356.
Payette, S., Delwaide, A., Caccianiga, M., Beauchemin, M., 2004. Accelerated thawing of subarctic peatland permafrost over the last 50 years. Geophys. Res. Lett. 31 (18).
Qian, B., Gregorich, E.G., Gameda, S., Hopkins, D.W., Wang, X.L., 2011. Observed soil temperature trends associated with climate change in Canada. J. Geophys. Res.-Atmos. 116, 1–16.
Qin, D., Jiao, C., Ding, Y., Yao, T., Bian, L., Jiawen, R.E.N., Wang, N., Liu, S., Diao, L., 2006. Progress on cryospheric studies by international and Chinese communities and perspectives. J. Appl. Meteorol. Sci. 17 (6), 649–656.
Qin, Y., Wu, T., Wu, X., Li, R., Xie, C., Qiao, Y., Hu, G., Zhu, X., Wang, W., Shang, W., 2017. Assessment of reanalysis soil moisture products in the permafrost regions of the central of the Qinghai–Tibet Plateau. Hydrol. Process. 31 (26), 4647–4659.
Rodell, M., Houser, P.R., Jambor, U., Gottschalck, J., Mitchell, K., Meng, C.J., Arsenault, K., Cosgrove, B., Radakovich, J., Bosilovich, M., Entin, J.K., Walker, J.P., Lohmann, D., Toll, D., 2004. The global land data assimilation system. Bull. Am. Meteorol. Soc. 85 (3), 381–394.
Romanovsky, V., Osterkamp, T., 1995. Interannual variations of the thermal regime of the active layer and near-surface permafrost in northern Alaska. Permafr. Periglac. Process. 6 (4), 313–335.
Romanovsky, V.E., Osterkamp, T.E., 1997. Thawing of the active layer on the coastal plain of the Alaskan Arctic. Permafr. Periglac. Process. 8 (1), 1–22.
Romanovsky, V.E., Drozdov, D.S., Oberman, N.G., Malkova, G.V., Kholodov, A.L., Marchenko, S.S., Moskalenko, N.G., Sergeev, D.O., Ukraintseva, N.G., Abramov, A.A., Gilichinsky, D.A., Vasiliev, A.A., 2010. Thermal state of permafrost in Russia. Permafr. Periglac. Process. 21 (2), 136–155.
Rusticucci, M.M., Kousky, V.E., 2002. A comparative study of maximum and minimum temperatures over Argentina: NCEP-NCAR reanalysis versus station data. J. Clim. 15 (15), 2089–2101.
Saha, S., Moorthi, S., Wu, X., Wang, J., Nadiga, S., Tripp, P., Behringer, D., Hou, Y.-T., Chuang, H.-Y., Iredell, M., Ek, M., Meng, J., Yang, R., Mendez, M.P., Van Den Dool, H., Zhang, Q., Wang, W., Chen, M., Becker, E., 2014. The NCEP climate forecast system version 2. J. Clim. 27 (6), 2185–2208.
Shiklomanov, N.I., Streletskiy, D.A., Nelson, F.E., Hollister, R.D., Romanovsky, V.E., Tweedie, C.E., Bockheim, J.G., Brown, J., 2010. Decadal variations of active-layer thickness in moisture-controlled landscapes, Barrow, Alaska. J. Geophys. Res. Biogeosci. 115, 1–14.
Shur, Y.L., Jorgenson, M.T., 2007. Patterns of permafrost formation and degradation in relation to climate and ecosystems. Permafr. Periglac. Process. 18 (1), 7–19.
Smith, S.R., Legler, D.M., Verzone, K.V., 2001. Quantifying uncertainties in NCEP reanalyses using high-quality research vessel observations. J. Clim. 14 (20), 4062–4072.
Tang, M., Sheng, Z., Chen, Y., 1979. On climatic characteristics of the Xizang Plateau monsoon. Acta Geograph. Sin. 34 (1), 34–42.
Toosi, E.R., Schmidt, J.P., Castellano, M.J., 2014. Soil temperature is an important regulatory control on dissolved organic carbon supply and uptake of soil solution nitrate. Eur. J. Soil Biol. 61, 68–71.
Trenberth, K.E., Fasullo, J.T., 2013. An apparent hiatus in global warming? Earth's Future 1 (1), 19–32.
Walvoord, M.A., Kurylyk, B.L., 2016. Hydrologic impacts of thawing permafrost-a review. Vadose Zone J. 15 (6), 20.
Wang, A., Zeng, X., 2012. Evaluation of multireanalysis products with in situ observations over the Tibetan Plateau. J. Geophys. Res.-Atmos. 117, 1–12.
Wang, S.L., Jin, H.J., Li, S.X., Zhao, L., 2000. Permafrost degradation on the Qinghai-Tibet Plateau and its environmental impacts. Permafr. Periglac. Process. 11 (1), 43–53.
Wang, G., Mao, T., Chang, J., Du, J., 2014. Impacts of surface soil organic content on the soil thermal dynamics of alpine meadows in permafrost regions: data from field observations. Geoderma 232, 414–425.
Wang, S., Zhang, M., Sun, M., Wang, B., Huang, X., Wang, Q., Feng, F., 2015. Comparison of surface air temperature derived from NCEP/DOE R2, ERA-Interim, and observations in the arid northwestern China: a consideration of altitude errors. Theor. Appl. Climatol. 119 (1–2), 99–111.
Wu, Q., Zhang, T., 2008. Recent permafrost warming on the Qinghai-Tibetan Plateau. J. Geophys. Res. 113 (D13), 1–22.
Wu, J., Sheng, Y., Wu, Q., 2009. Processes and modes of permafrost degradation on the Qinghai-Tibet Plateau. Science in China. Series D. Earth Sci. 39 (11), 1570–1578.
Wu, X., Zhao, L., Hu, G., Liu, G., Li, W., Ding, Y., 2017. Permafrost and land cover as controlling factors for light fraction organic matter on the southern Qinghai-Tibetan plateau. Sci. Total Environ. 613-614, 1165–1174.
Wu, X., Nan, Z., Zhao, S., Zhao, L., Cheng, G., 2018. Spatial modeling of permafrost distribution and properties on the Qinghai-Tibet Plateau. Permafr. Periglac. Process. 29, 86–99.
Xiao, Y., Zhao, L., Dai, Y., Li, R., Pang, Q., Yao, J., 2013. Representing permafrost properties in CoLM for the Qinghai-Xizang (Tibetan) Plateau. Cold Reg. Sci. Technol. 87, 68–77.
Xie, C., Zhao, L., Wu, J., Qiao, Y., 2010. Features and changing tendency of the permafrost

in Mahan Mountain, Lanzhou. J. Glaciol. Geocryol. 32 (5), 883–890.
Yanai, M., Wu, G.X., 2006. Effects of the Tibetan. Plateau 29 (5), 513–549.
Ye, D., Gao, Y., 1979. The Meteorology of the Qinghai-Xizang (Tibet) Plateau. Science Press, Beijing, pp. 278.
Yesilirmak, E., 2014. Soil temperature trends in Buyuk Menderes Basin, Turkey. Meteorol. Appl. 21 (4), 859–866.
You, Q., Fraedrich, K., Ren, G., Ye, B., Meng, X., Kang, S., 2012. Inconsistencies of precipitation in the eastern and central Tibetan Plateau between surface adjusted data and reanalysis. Theor. Appl. Climatol. 109 (3–4), 485–496.
You, Q., Jiang, Z., Wang, D., Pepin, N., Kang, S., 2017. Simulation of temperature extremes in the Tibetan Plateau from CMIP5 models and comparison with gridded observations. Clim. Dyn. 4, 1–15.
Yu, W., Zhou, S., Wang, W., 2003. Specifications for Surface Meteorological Observation. China Meteorological Press, Beijing, China.
Zhang, T., Barry, R.G., Gilichinsky, D., Bykhovets, S.S., Sorokovikov, V.A., Ye, J.P., 2001. An amplified signal of climatic change in soil temperatures during the last century at Irkutsk, Russia. Clim. Chang. 49 (1–2), 41–76.
Zhang, Y., Chen, W., Smith, S., Riseborough, D., Cihlar, J., 2005. Soil temperature in Canada during the twentieth century: complex responses to atmospheric climate change. J. Geophys. Res.-Atmos. 110 (D3), 1–15.
Zhang, W., Li, S., Pang, Q., 2008. Variation characteristics of soil temperature over Qinghai-Xizang Plateau in the past 45 years. Acta Geograph. Sin. 63 (11), 1151–1159.
Zhao, L., Cheng, G., Li, S., Zhao, X., Wang, S., 2000. Thawing and freezing processes of active layer in Wudaoliang region of Tibetan Plateau. Chin. Sci. Bull. 45 (23), 2181–2187.
Zhao, L., Ping, C.L., Yang, D.Q., Cheng, G.D., Ding, Y.J., Liu, S.Y., 2004. Changes of climate and seasonally frozen ground over the past 30 years in Qinghai-Xizang (Tibetan) Plateau, China. Glob. Planet. Chang. 43 (1–2), 19–31.
Zhao, R.-X., Wu, G.-X., Zhang, H., 2008. Seasonal characteristic and interannual variability of the atmospheric hydrological cycle in the Yangtze River basin during the summer monsoon period. Chin. J. Geophys. 51 (6), 1670–1681 (Chinese Edition).
Zhao, L., Wu, Q., Marchenko, S., Sharkhuu, N., 2010. Thermal state of permafrost and active layer in Central Asia during the international polar year. Permafr. Periglac. Process. 21 (2), 198–207.
Zhao, L., Li, R., Ding, Y., Xiao, Y., Sun, L., Liu, Y., 2011. Soil thermal regime in Qinghai-Tibet plateau and its adjacent regions during 1977–2006. Adv. Clim. Chang. Res. 7 (5), 307–316.
Zhao, L., Wu, T., Xie, C., Li, R., Wu, X., Yao, J., Yue, G., Xiao, Y., 2017. Support geoscience research, environmental management, and engineering construction with investigation and monitoring on permafrost in the Qinghai-Tibet Plateau, China. Bull. Chin. Acad. Sci. 32 (10), 1159–1168.
Zhou, L., Du, Z., 2016. Regional differences in the surface energy budget over China: an evaluation of a selection of CMIP5 models. Theor. Appl. Climatol. 124 (1–2), 241–266.
Zhou, Y., Guo, D., Qiu, G., Cheng, G., Li, S., 2000. China Permafrost. Science Press, Beijing.
Zhu, X., Liu, Y., Wu, G., 2012. An assessment of summer sensible heat flux on the Tibetan Plateau from eight data sets. Sci. China Earth Sci. 55 (5), 779–786.
Zhu, F., Cuo, L., Zhang, Y., Luo, J.-J., Lettenmaier, D.P., Lin, Y., Liu, Z., 2017. Spatiotemporal variations of annual shallow soil temperature on the Tibetan Plateau during 1983–2013. Clim. Dyn. 1–19.
Zou, H., Zhu, J., Zhou, L., Li, P., Ma, S., 2014. Validation and application of reanalysis temperature data over the Tibetan Plateau. J. Meteorol. Res. 28 (1), 139–149.
Zou, D., Zhao, L., Sheng, Y., Chen, J., Hu, G., Wu, T., Wu, J., Xie, C., Wu, X., Pang, Q., Wang, W., Du, E., Li, W., Liu, G., Li, J., Qin, Y., Qiao, Y., Wang, Z., Shi, J., Cheng, G., 2017. A new map of permafrost distribution on the Tibetan Plateau. Cryosphere 11 (6), 2527–2542.